Micro-arcing in a helicon plasma reactor

J Ling, R W Boswell, T Lafleur, and C Charles

Space Plasma, Power and Propulsion Group, Research School of Physics and Engineering, Australian National University, ACT 0200, Australia

E-mail: `julia.ling@anu.edu.au`

Abstract.

Micro-arcing is investigated with a helicon plasma reactor in an argon plasma using a Langmuir probe to measure the plasma floating potential during arc events and a stainless steel probe arm on which micro-arcs occurred to measure the current flow during micro-arc events. The frequency of spark events was analyzed with varying rf powers and pressures, and was found to depend strongly on the plasma floating potential. The micro-arcs were shown to cause a drop in the bulk floating potential that lasted on the order of hundreds of microseconds to milliseconds. During this period, a current on the order of an ampere was found to flow to the site of the spark event, leading to a total charge flow of on the order of 10^{-3} C.

PACS numbers: 50.20.Nr, 52.80.Mg, 52.80.Pi

1. Introduction

Micro-arcs, sometimes informally referred to as "sparks," are present in many helicon plasma reactors, and can induce serious problems including contamination of the plasma with sputtered ions from the chamber walls, damage to sensitive electronics, and unpredictability of bulk plasma properties. Dc electrical breakdown has been studied for decades. The Fowler-Nordheim theory of cold electron emission from metals, presented in 1928, formed the theoretical foundation for how breakdown could occur from cathodic electron emission [1]. Cranberg suggested that breakdown was initiated by a "clump" of the cathode (or, less commonly, anode) becoming separated from the rest and impinging on the electrode of opposite voltage, thereby causing localized vaporization and breakdown [2]. Since then, many more investigations into the dc electrical breakdown mechanism have been performed [3, 4, 5, 6].

However, the mechanism for these micro-arcs in rf discharges is poorly understood. A previous study by Yin *et al* measured the floating potential during micro-arc events in rf hollow-cathode plasmas, and showed that increasing plasma floating potential is associated with increased micro-arc frequency [7]. This paper will investigate micro-arc events in a helicon plasma reactor. Previous work on this reactor revealed the presence of a low-magnetic field mode (at 25 G peak on-axis magnetic field) that was associated with increased ion density ($\approx 10^{17}\ m^{-3}$ in the source region) and increased plasma potential (≈ 60 V in the diffusion chamber) [8]. At higher rf powers (above 450 W rf), micro-arcs were observed in the diffusion chamber in the low-magnetic field mode. To investigate the nature of these micro-arcs, the magnetic field was maintained at 25 G, such that the plasma remained in the low-magnetic field mode throughout the course of these measurements.

2. Experimental Set-up

2.1. Experimental apparatus

The experimental apparatus consists of a source region housed inside a larger vacuum chamber. The Pyrex source tube is 5 mm thick, 29 cm long, has an outer diameter of 15 cm, and is closed on one end. The source tube axis will be taken as the z-axis, with the positive direction extending out of the open end of the source tube and the origin set at the source tube exit. The gas inlet is located in the center of the closed end of the source tube. An 18 cm long helicon double-saddle field antenna is wrapped around the source tube. The antenna is copper with a 1 mm thick boron-nitride coating, and is operated at 13.56 MHz. The antenna impedance matching network is located outside the vacuum chamber, and consists of two tunable vacuum capacitors in an L-configuration, along with a blocking capacitor to isolate the antenna from ground. Two solenoids are wrapped co-axially around the source tube and create a magnetic field that is relatively constant within the source region, but which diverges sharply at the exit. The source tube is mounted within a 1 m diameter by 1.4 m long stainless steel

vacuum chamber as shown in figure 1. The vacuum chamber has a base pressure of 10^{-6} Torr, maintained by a turbomolecular pump in conjunction with a rotary pump. The pressure was measured by a Granville-Phillips Series 274 ionization gauge and a MKS 22CA barotron gauge, and, due to a low ionization fraction ($\approx 1\%$), did not change significantly when the plasma was ignited.

2.2. Probe design

Two probe diagnostics were used to collect the data presented in this paper. The first was an uncompensated planar disc Langmuir probe that was connected directly to an oscilloscope to take time-resolved measurements of the plasma floating potential. The Langmuir probe had a probe tip diameter of 3 mm and was installed axially along the z-axis. Because the impedance of the oscilloscope was 1 MΩ, the RC time constant of this measurement circuit was found to be on the order of tens of microseconds, which is comparable to the length of the micro-arc event. Therefore, to achieve time resolution on the order of microseconds, the Langmuir probe could be connected to ground through a 100 kΩ resistor. However, floating potential measurements taken with this 100 kΩ resistor in place show a much lower "floating potential," as the Langmuir probe is no longer truly floating. As such, floating potential measurements taken with the 100 kΩ resistor in place give only a time-resolved relative measure of the floating potential during micro-arc events, and will not agree quantitatively with the true floating potential measurements taken without the 100 kΩ resistor.

The second diagnostic used, a "current probe," consisted of a 0.5 m long stainless steel tube, 0.6 cm in diameter. This tube was installed radially in the vacuum chamber at z=10 cm, and could be pushed and pulled in and out of the plasma column at will. When the probe was inserted into the plasma, micro-arc events could occur on it. The probe was connected to ground through a 1 Ω $\pm 5\%$ 1 Watt metal film resistor. The voltage drop over the 1 Ω resistor could be measured to determine the current flow to the current probe during a micro-arc event. The time constant of this measurement system was found to be on the order of tens of nanoseconds, comparable to the time-resolution of the oscilloscope, and far shorter than the time constants measured during the micro-arc events.

Lastly, a Casio Ex-F1 camera was used to take photographs of the micro-arc events at frame rates of 1200 fps with a resolution of 336 by 96 pixels. This camera was directed at the current probe to investigate the temporal evolution of the micro-arcs.

3. Results and Discussion

The floating potential was measured during micro-arc events by connecting the Langmuir probe, positioned at z=16 cm, straight to the oscilloscope. Figure 2 shows a typical example of the floating potential variation during a micro-arc event. The floating potential starts at 30 V, then dips at the inception of the spark to approximately 5 V,

remaining low for almost a millisecond before rebounding to near its previous value. The final floating potential rebuilds to the initial floating potential on the order of milliseconds. It should be remembered that since the time constant of the measurement circuit is in the tens of microseconds, the decay and recovery times for the floating potential are not necessarily accurate. As can be seen in figure 2, the rf noise on the floating potential signal decreased significantly during the micro-arc event; this same effect was observed with all the measurements taken with the Langmuir probe. The micro-arc event associated with the observed dip in floating potential occurred on the vacuum chamber wall, at a distance of greater than 0.5 m from the Langmuir probe tip, indicating that the micro-arc event causes a system-wide collapse in floating potential.

The floating potential before and during micro-arcs was recorded as a function of rf power at 0.3 mTorr argon, with the Langmuir probe at z=16 cm. At each parameter space, ten sparks were recorded and the floating potentials were averaged over these ten events. The results are shown in figure 3, with the error bars corresponding to the standard deviation of the data from the ten events. As figure 3 reveals, although the plasma floating potential rises with increasing rf power, the minimum floating potential occurring during the spark remains relatively constant. The large error bars recorded at 520 W rf power were due to the instability of the plasma at that power level. The duration of micro-arcs was analyzed and found to remain relatively constant with varying rf power at 1.0 ± 0.5 ms.

The micro-arc frequency was measured with varying argon pressure and rf power. The frequency was calculated by recording the number of dips seen in the floating potential as measured by the Langmuir probe at z=16 cm during a 10 s period. This number of events was then divided by 10 to yield the spark frequency in Hertz. At each parameter set, the background (i.e. not during a micro-arc event) floating potential was also measured. The spark frequency with increasing argon pressure is shown in figure 4, with the floating potentials overlaid for comparison. As can be seen in figure 4, both the spark frequency and the plasma floating potential decrease with increasing pressure.

The spark frequency and floating potential are also measured with increasing rf power, at a constant pressure of 0.3 mTorr argon, as shown in figure 5. Figure 5 shows that the floating potential and spark frequency both rise with increasing rf power. To investigate the correlation between floating potential and spark frequency, figure 6 shows the spark frequency plotted versus plasma floating potential for both of the cases discussed above: constant rf power and increasing pressure, and constant pressure with increasing rf power. As can be seen in figure 6, while the spark frequency does rise with increasing floating potential in both cases, the two cases do not match perfectly, indicating that the spark frequency also has a dependence on other factors besides the floating potential. Perhaps the true dependence of the spark frequency is on the plasma potential; however, due the relative difficulty of taking time-resolved plasma potential measurements, the floating potential was measured here instead. Yin *et al* have also reported a rise in spark frequency with increasing floating potential in their rf hollow-cathode system [7].

The precipitous drop in floating potential that occurs during a micro-arc event indicates a flow of current to the surface on which the spark occurs. Previous investigations into this current flow are scant; however, by inserting a metal probe into the plasma and allowing micro-arcs to occur on its surface, this current flow was easily measured. Data was taken simultaneously with the current probe at z=10 cm and with the Langmuir probe at z=20 cm. To achieve greater time resolution with the Langmuir probe for better comparison to the current probe data, the Langmuir probe was connected to ground through a 100 kΩ resistor; as a result, the floating potentials measured were significantly lower. Nonetheless, the qualitative trends in the data remain the same: a dip in floating potential is still seen at the start of the micro-arc, and lasts on the order of hundreds of microseconds. Figure 7 shows that the dip in floating potential as measured by the Langmuir probe corresponds to a current flow to the current probe of the same duration and of a magnitude on the order of Amps. The lag between the initial rise in current on the current probe and the fall in the floating potential was measured to be less than 5 μs, corresponding to a signal speed in the plasma of greater than 20 km/s, far greater than the Bohm velocity. It therefore seems as if the signal within the plasma must be carried by the electrons, not the ions.

The current flow during the micro-arc event is marked by three distinct phases: the rise, the gradual decay, and the sudden cut-off of the current. The current rise time has been measured to be approximately 10-20 μs, the gradual decay of the current lasts on the order of hundreds of microseconds, and the sudden cut-off lasts less than a microsecond. The mechanism that determines these times scales and the sudden current cut-off is as yet unknown, and is the focus of ongoing research.

From the current probe data, the total charge flow during a micro-arc event can be calculated by numerically integrating the current flow during the event. Because there was some small ($<$ 0.05 A) current flow to the probe even when a spark was not occurring on the probe, this "background" current was measured and subtracted from the current flow during the micro-arc before the numerical integration calculation. Measurements were taken at 0.3 mTorr argon for varying rf powers, with five measurements taken at each parameter space. Figure 8 shows the mean total charge flow, with the standard deviation of the total charge flow for the five measurements providing the error bars. As figure 8 reveals, the total charge flow increases with increasing rf power, and is on the order of a milli-Coulomb. This total charge flow is several orders of magnitude larger than the charge excess that exists in the plasma in equilibrium. However, it must be remembered that the system-wide collapse in the floating potential will cause an increased electron flux to the vacuum chamber walls, such that the flow of current to the site of the spark could be partially balanced by a net electron current flowing to the walls at every other site in the chamber.

A camera was operated at 1200 fps and focused on the current probe such that it was able to capture the development of a particularly long-duration micro-arc that lasted approximately 4 ms. The photographs, shown in figure 9, reveal that the micro-arc moved approximately 5 cm along the surface of the probe arm (which extends

horizontally across the images). Photographic series were also taken of several other micro-arc events and confirmed that the micro-arcs would often move along the probe surface. The progression of the micro-arcs along the surface of the probe arm suggests that the surface material could be playing a critical role in the micro-arc process.

The mechanism behind the micro-arc events is an area of ongoing research. Yin *et al* attributed the formation of micro-arcs to field emission from the chamber walls [7]. Townsend breakdown seems like an unlikely mechanism in the system used for this study, because argon ionization within the wall sheath should be minimal: the mean free path for ionization is on the order of meters, whereas the sheath width for the plasmas in this study is on the order of millimeters.

However, these micro-arcs do bear a striking resemblance to cathodic arcs, which are characterized by high currents (typically tens of Amperes) over low voltage drops (less than 100 V) [9, 10, 11]. Cathodic arcs are typically initiated by a mechanical trigger that short-circuits the anode to the cathode, starting an explosive electron emission process that arises due to a synergy of high electric fields, high temperature, and cathode ionization [11, 12]. A positive feedback loop develops as localized electron field emission at points of surface roughness causes Ohmic heating, which in turn induces a greater rate of electron emission from the cathode surface [10, 11]. The temperature of the cathode surface can rise enough to vaporize the surface, leading to the creation of a dense plasma near the cathode surface. This high density plasma reduces the plasma sheath width, increasing the localized electric field and the associated field emission, which causes the formation of a cathode spot [11]. The cathodic arc propagates by the sequential creation of daughter spots at the edge of extinguishing parent spots [9, 10], giving the arc the appearance of "moving" along the surface of the cathode. The cathodic arc has a characteristic "chopping current" below which the electron emission and surface vaporization rates are not great enough to sustain the dense plasma near the cathode and the arc spontaneously extinguishes [10, 13, 14].

The cathodic arc shares several similarities with the micro-arc phenomenon described in this paper: it exhibits high current densities over low voltage drops, the current has a fast rise time and sudden cut-off at the end of the arc, and the arc propagates along the surface, leaving behind a trail of roughened surface. (These trails were observed in this system on the surface of the current probe.) Although the micro-arc ignition in the absence of a mechanical trigger is a notable difference between these two types of arcs, these phenomenological similarities indicate that the micro-arc mechanism in this rf system could share some aspects of the dc cathodic arc mechanism.

4. Conclusion

Floating potential measurements made during micro-arc events have shown that the floating potential decreases during the sparks, and remains low for hundreds of microseconds. The frequency of the sparks increased with increasing rf power and decreasing pressure, and seemed strongly correlated to the plasma floating potential.

For the first time in a helicon plasma source, the current flow during a micro-arc event is reported. The current flow was characterized by three distinct phases: a fast rise in current, followed by a slow decay and an eventual sudden cut-off. It was found that the current flow was of the same duration as the dip in floating potential and had a magnitude on the order of Amperes. The total charge flow during the micro-arc events was shown to increase with rf power, and was on the order of milli-Coulombs. Although the micro-arc mechanism remains unclear, the data presented in this paper suggest that the high current flow and charge transfer make the micro-arc events a definite risk for any sensitive electronics or diagnostics within the plasma. Furthermore, by lowering the floating potential (which can be accomplished by modulating the pressure or input power), this problem can be mitigated.

Acknowledgments

Julia Ling was supported by an American Australian Association Education Fellowship, and would like to thank the SP3 group for hosting her during her stay in Australia.

References

[1] R H Fowler and L Nordheim. *Proc. R. Soc. Lond.*, 124:699, 1928.
[2] L Cranberg. *J. Appl. Phys.*, 23:518, 1951.
[3] W P Dyke and J P Trolan. *Phys. Rev.*, 89:799, 1953.
[4] J M Somerville. *The Electric Arc.* Methuen and Co, London, 1959.
[5] J A Rees. *Electrical Breakdown in Gases.* Macmillan Press, London, 1973.
[6] I Safi. *Surf. Coat. Technol.*, 127:203, 2000.
[7] Y Yin, MM Bilek, D R McKenzie, R W Boswell, and C Charles. *J. Phys. D: Appl. Phys.*, 37:2871, 2004.
[8] J Ling, M D West, T Lafleur, C Charles, and R W Boswell. *J. Phys. D: Appl. Phys.*, 43, 2010.
[9] L R Boxman and S Goldsmith. *Surface and Coatings Technology*, 33:153, 1987.
[10] I G Brown. *Annu. Rev. Mater. Sci.*, 28:243, 1998.
[11] A Anders. *Thin Solid Films*, 502:22, 2005.
[12] A J Perry and J N Mattosian. *Metallurgical and Materials Transactions A*, 29A:593, 1998.
[13] R P P Smeets. *Low-current behavior and current chopping of vacuum arcs.* PhD thesis, 1987.
[14] P G Slade. *The vacuum interrupter: theory, design and application.* 2008.
[15] M D West, C Charles, and R W Boswell. *J. Prop. and Power*, 24:134, 2008.

Figure captions

Figure (1) A cross-sectional schematic of helicon plasma system used in these experiments showing the Pyrex source tube (A), antenna feedthroughs (B), the propellant feedline (C), solenoid coils (D), RFEA (E) and Langmuir probe (F). [15]
Figure (2) An example of the floating potential during a typical micro-arc event, as measured by a Langmuir probe at z=16 cm, 470 W rf power, 0.3 mTorr argon. The micro-arc event begins at t=0 ms, and lasts approximately 1 ms.
Figure (3) Floating potential measurements taken by a Langmuir probe at z=16 cm, 0.3 mTorr argon for varying rf powers before (circles) and during (stars) a micro-arc event. The potential during the micro-arc is taken to be the minimum potential reached during the event.
Figure (4) Micro-arc frequency (circles, left axis) and plasma floating potential at z= 16 cm (stars, right axis) as a function of argon pressure at 580 W rf.
Figure (5) Micro-arc frequency (circles, left axis) and plasma floating potential at z=16 cm (stars, right axis) as a function of rf power at 0.3 mTorr argon.
Figure (6) Micro-arc frequency as a function of floating potential, as measured with 580 W rf and varying pressure (circles), and 0.3 mTorr argon with varying rf power (stars).
Figure (7) The current flow (a), and floating potential measured over a 100 kΩ resistor (b), during a micro-arc event at 410 W rf, 0.3 mTorr.
Figure (8) The total charge flow during micro-arc events as measured by the current probe at 0.3 mTorr argon with varying rf powers.
Figure (9) Photographs of a micro-arc progressing along the current probe arm, taken at 1200 fps. The spark ignites (a), and then moves along the probe arm (b-e) before extinguishing (f).

Figure 1.

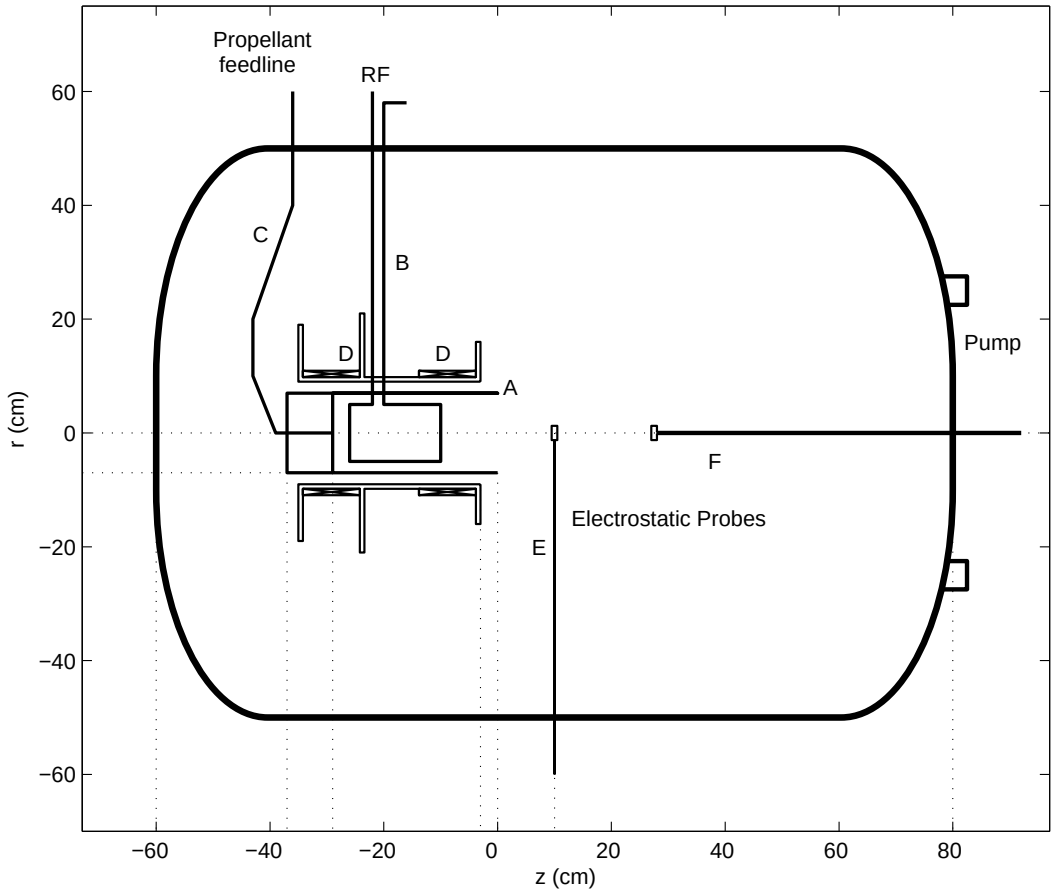
Propellant
feedline
RF
C
B
D
D
A
Pump
F
Electrostatic Probes
E
r (cm)
z (cm)
60
40
20
0
−20
−40
−60
−60
−40
−20
0
20
40
60
80

Figure 2.

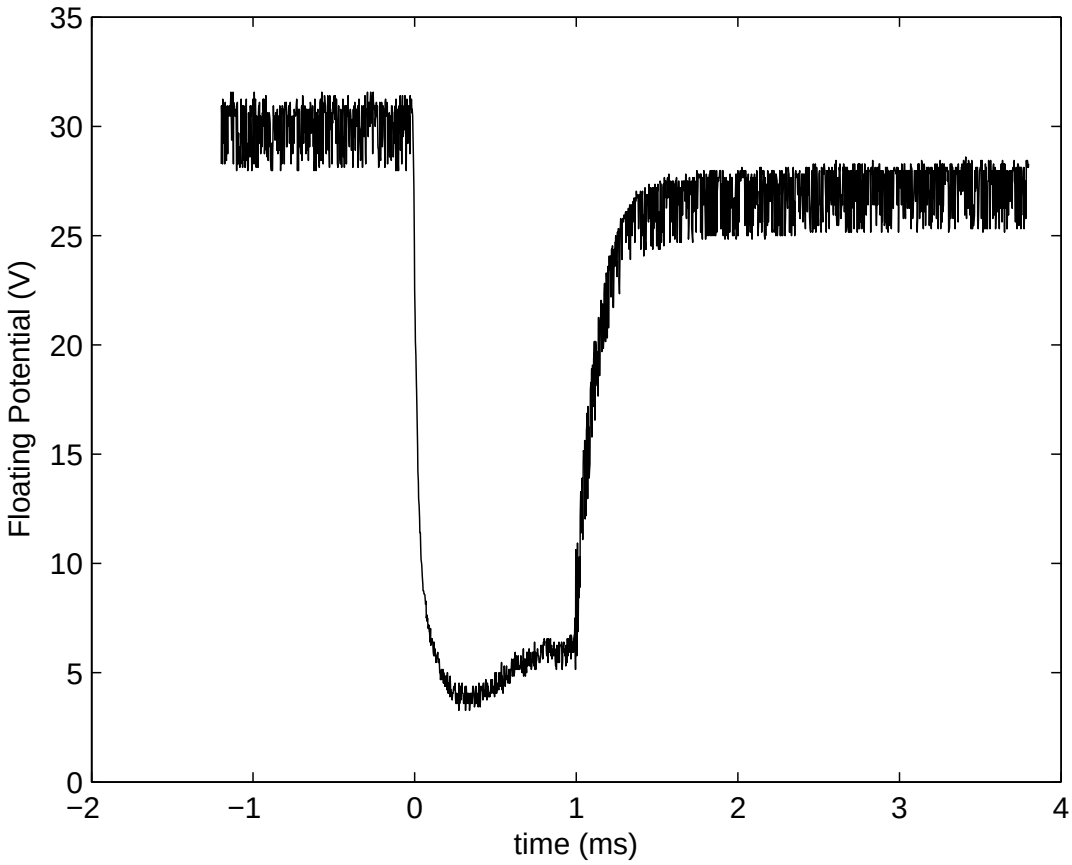

Figure 3.

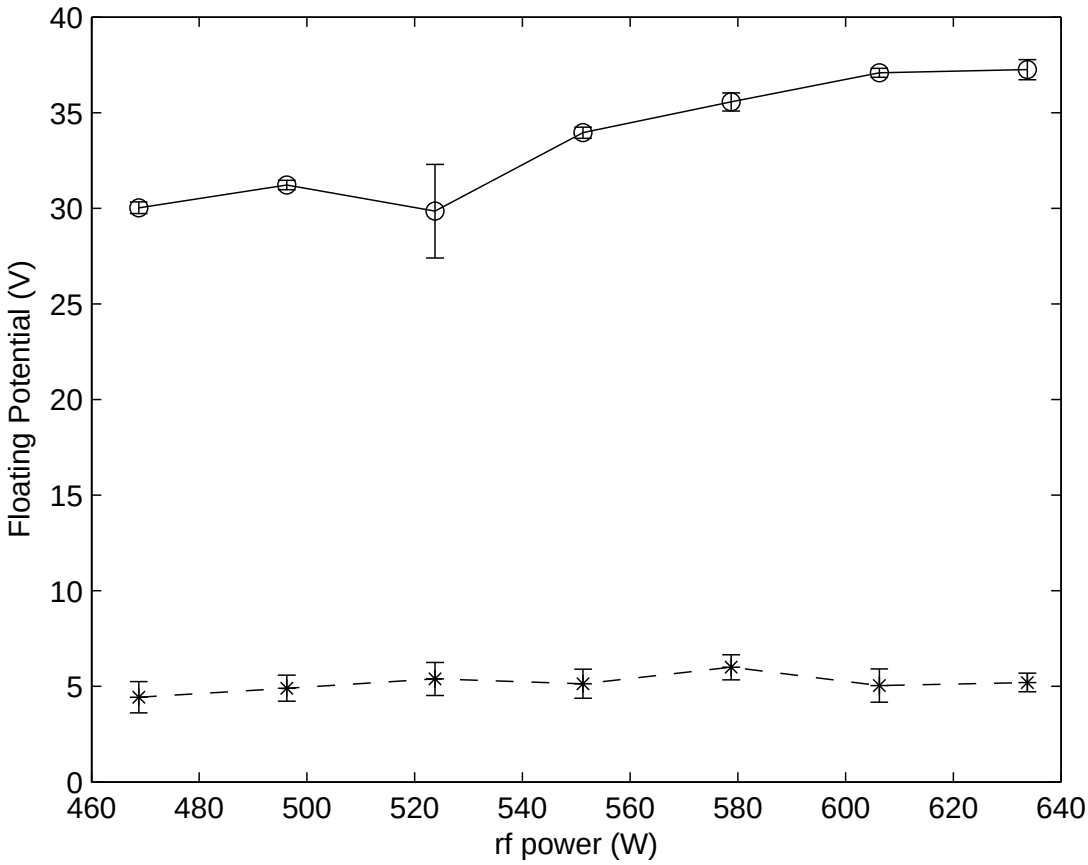
Floating Potential (V)
rf power (W)
0
5
10
15
20
25
30
35
40
460
480
500
520
540
560
580
600
620
640

Figure 4.

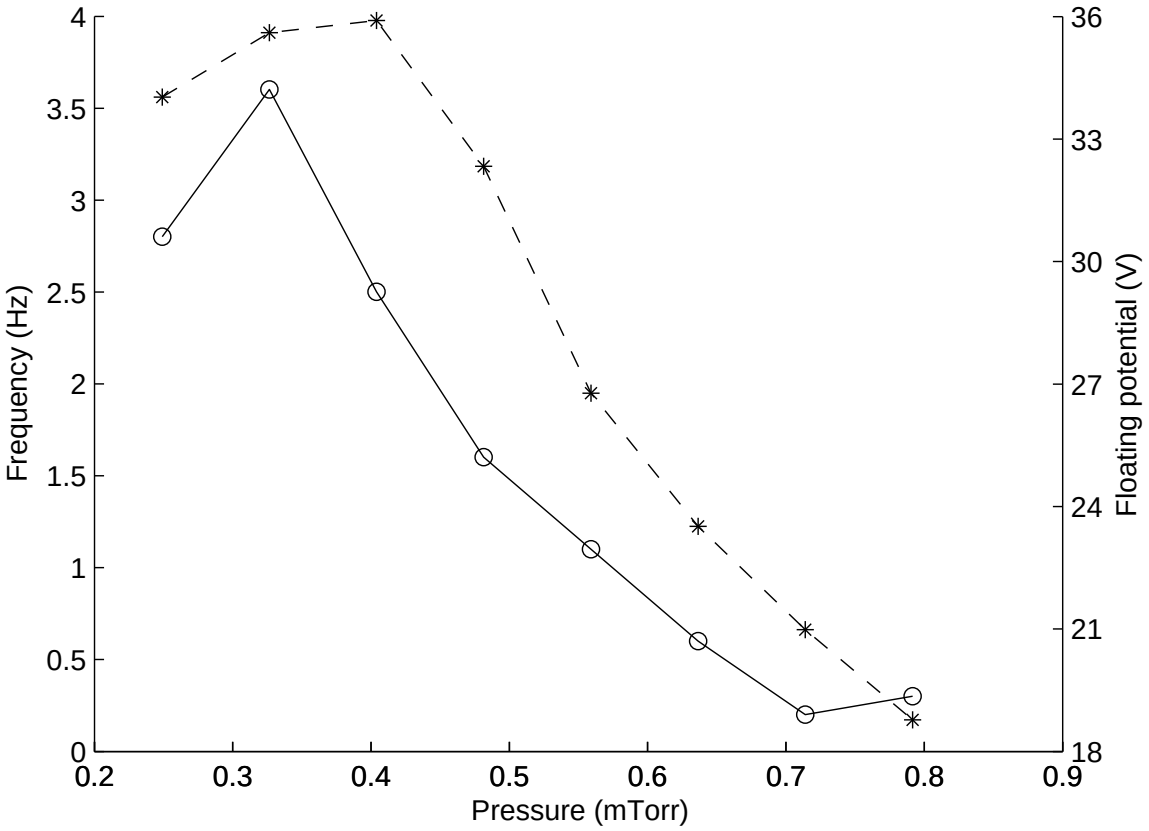
Frequency (Hz)
Floating potential (V)
Pressure (mTorr)
0
0.5
1
1.5
2
2.5
3
3.5
4
18
21
24
27
30
33
36
0.2
0.3
0.4
0.5
0.6
0.7
0.8
0.9

Figure 5.

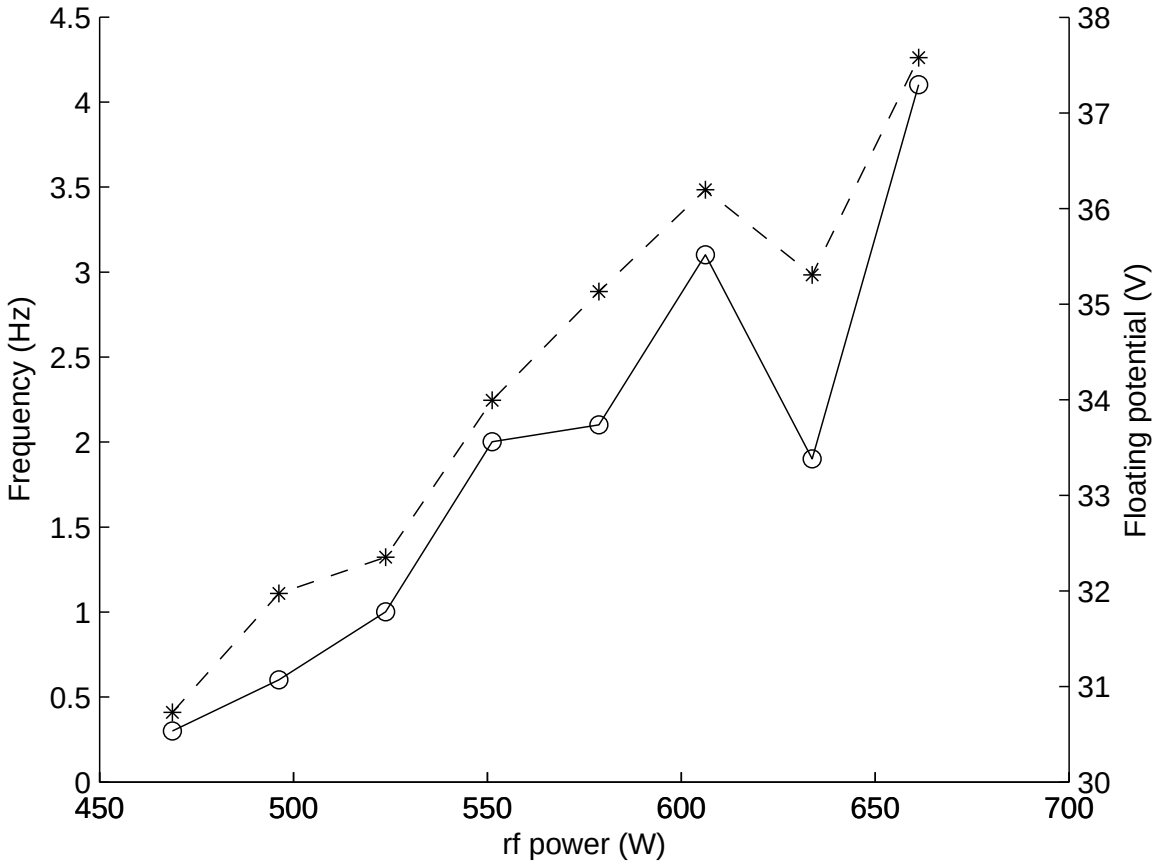
Frequency (Hz)
Floating potential (V)
rf power (W)
0
0.5
1
1.5
2
2.5
3
3.5
4
4.5
30
31
32
33
34
35
36
37
38
450
500
550
600
650
700

Figure 6.

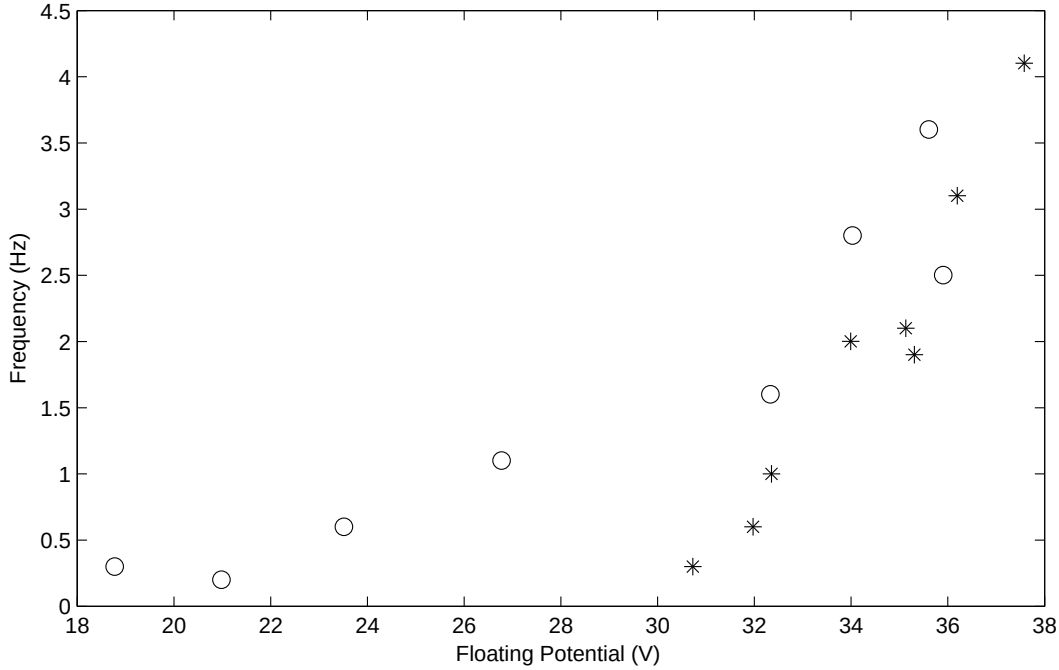
Frequency (Hz)
Floating Potential (V)
0
0.5
1
1.5
2
2.5
3
3.5
4
4.5
18
20
22
24
26
28
30
32
34
36
38

Figure 7.

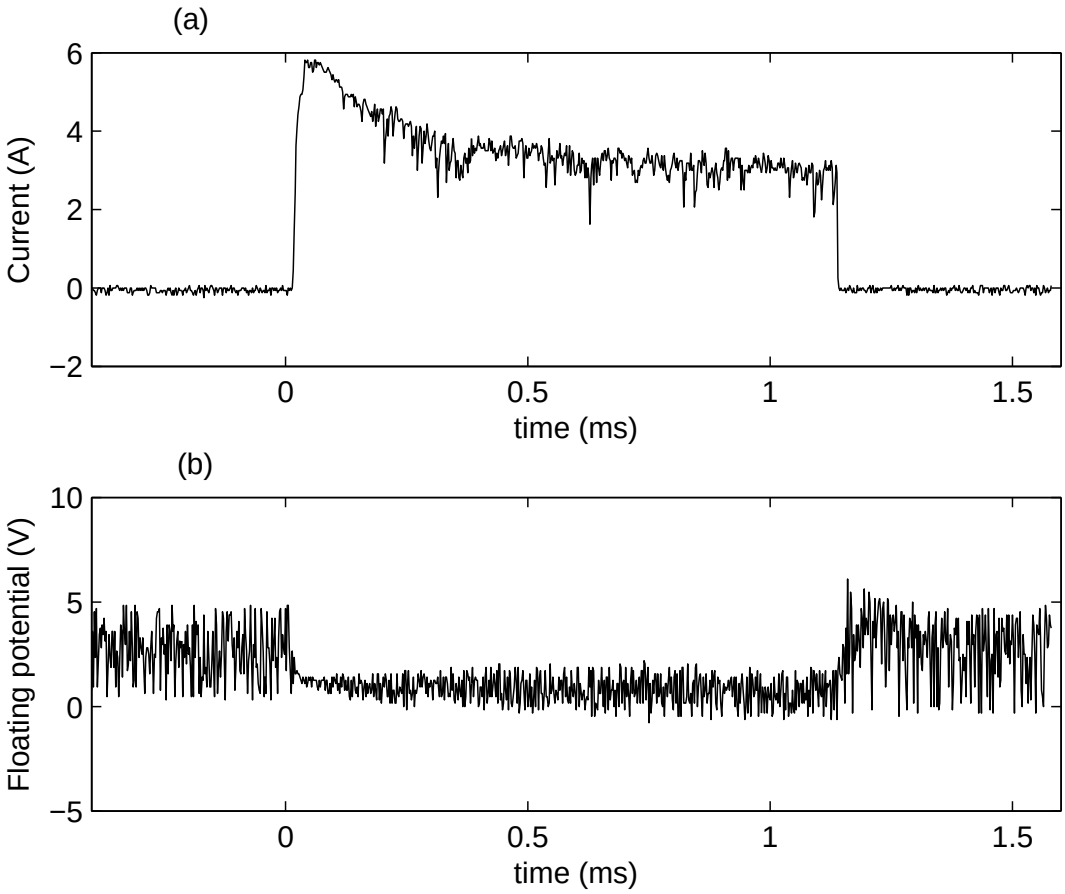
(a)
Current (A)
6
4
2
0
−2
0
0.5
1
1.5
time (ms)
(b)
Floating potential (V)
10
5
0
−5
0
0.5
1
1.5
time (ms)

Figure 8.

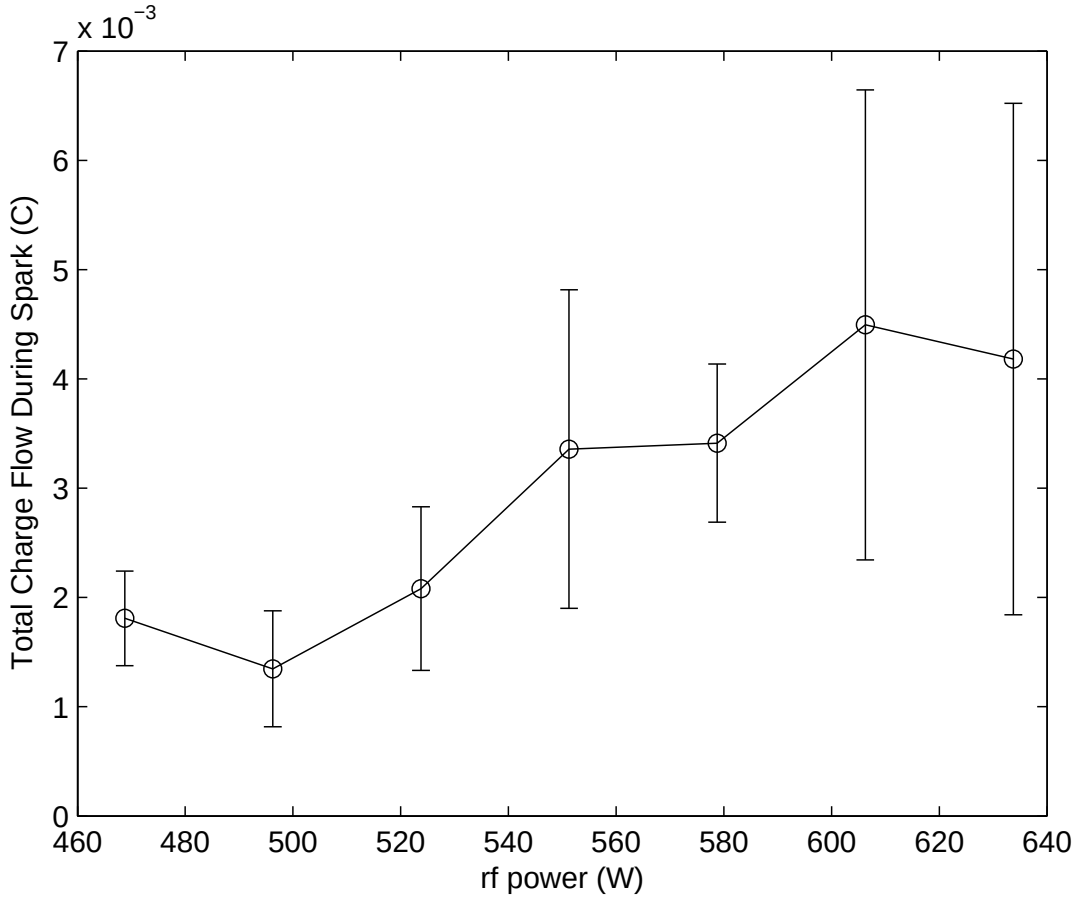
x 10^−3
7
6
5
4
3
2
1
0
Total Charge Flow During Spark (C)
460
480
500
520
540
560
580
600
620
640
rf power (W)

Figure 9.